# Self-Assembled Fibrinogen Scaffolds Support Cocultivation of Human Dermal Fibroblasts and HaCaT Keratinocytes

Arundhati Joshi, Titinun Nuntapramote, and Dorothea Brüggemann*

ACCESS | 📊 Metrics & More | 📖 Article Recommendations | 🔲 Supporting Information

**ABSTRACT:** Self-assembled fibrinogen scaffolds are highly attractive biomaterials to mimic native blood clots. To explore their potential for wound healing, we studied the interaction of cocultures of human dermal fibroblasts (HDFs) and HaCaT keratinocytes with nanofibrous, planar, and physisorbed fibrinogen. Cell viability analysis indicated that the growth of HDFs and HaCaTs was supported by all fibrinogen topographies until 14 days, either in mono- or coculture. Using scanning electron microscopy and cytoskeletal staining, we observed that the native morphology of both cell types was preserved on all topographies. Expression of the marker proteins vimentin and cytokeratin-14 showed that the native phenotype of fibroblasts and undifferentiated keratinocytes, respectively, was maintained. HDFs displayed their characteristic wound healing phenotype, characterized by expression of fibronectin. Finally, to mimic the multilayered microenvironment of skin, we established successive cocultures of both cells, for which we found consistently high metabolic activities. SEM analysis revealed that HaCaTs arranged into a confluent top layer after 14 days, while fluorescent labeling confirmed the presence of both cells in the layered structure after 6 days. In conclusion, all fibrinogen topographies successfully supported the cocultivation of fibroblasts and keratinocytes, with fibrinogen nanofibers being particularly attractive for skin regeneration due to their biomimetic porous architecture and the technical possibility to be detached from an underlying substrate.
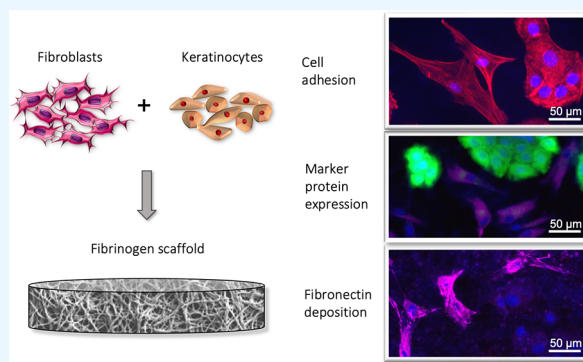
## 1. INTRODUCTION

Impaired wound healing is often associated with chronic wounds, which represent a major clinical challenge for skin regeneration,[1−3] with the inability or absence of re-epithelialization serving as a vital indicator.[4,5] Various tissue engineering approaches have significantly improved skin therapeutics in recent years, for instance, 3D bioprinting of cell-laden constructs, hydrogel systems with embedded cells, multicellular spheroids, and organ-on-a-chip technology.[1,6−8] Yet, disadvantages of these methods include complex manufacturing processes, batch-to-batch inconsistencies, or difficulties in nutrient supply.[6]

Advanced approaches for *in situ* regeneration of skin tissue therefore utilize engineered cell-free bioresponsive scaffolds[9] that channel the innate regenerative ability of the body to recruit endogenous cells to the wound site.[10] In the native three-layered skin, keratinocytes form the main cellular component of the upper epidermis, and the lower dermis is infiltrated by fibroblasts.[11] Based on numerous soluble factors, there is a strong crosstalk between both cell types,[12] and along with endothelial cells they regulate complex events during skin repair via cell−cell communication.[2,13] Due to the complex architecture of native skin, new scaffold materials for skin regeneration need to support the cocultivation of different cell types,[6] thereby providing a matrix that mimics the micro-

environment of the native three-layered skin structure as closely as possible.[14] The first coculture systems for skin repair were developed in the 1990s and focused on fibroblasts and keratinocytes, while later fibroblasts and endothelials were cocultivated to study the effect of vascularization.[15] Prevascularization is an essential aspect also for other areas of tissue engineering, which require the development of new coculture systems and biomaterials[16] that have the potential to be shaped into tubular scaffolds.[17]

The adhesive glycoprotein fibrinogen is very well-suited for skin tissue engineering[18] since it provides important cell adhesion sites for fibroblasts, endothelial cells, and blood platelets via integrins[19,20] as well as a high binding affinity for various growth factors.[21] Such biochemical cues can be used to activate specific signaling pathways to control cellular responses and facilitate the homing of endogenous cells.[10] In addition, biophysical properties of tissue-engineered scaffolds

such as the porous architecture are important in facilitating revascularization, as an interconnected porous network facilitates cellular infiltration, tissue ingrowth, and extracellular matrix (ECM) deposition.[10,22] In particular, fibrinogen fibers can promote wound healing by mimicking the biochemical composition and nanofibrous architecture of native blood clots.[18,21,23] Similarly, fibrin hydrogels, obtained by thrombin-mediated cleavage of fibrinogen,[24] have been used as biological wound healing scaffolds[23] that enable cocultivation of keratinocytes and fibroblasts.[25,26] Yet, these hydrogels often suffer from substantial shrinkage and fast degradation[27] and require the addition of enzymes and other polymers to optimize their mechanical strength or resistance to fibrinolysis, which increases their production time and costs.[18,28]

Alternatively, electrospun fibrinogen nanofibers can mimic the porous 3D nanoarchitecture of the ECM and native blood clots,[29,30] as well as provide bioactive cues, which electrospun nanofibers prepared from synthetic polymers lack[31] unless additionally conditioned with ECM components.[32] So far, electrospun fibrinogen nanofibers were found to promote growth of fibroblasts,[30,33,34] endothelial cells,[35] smooth muscle cells,[36] and mesenchymal stem cells.[37,38] Even so, electrospinning usually requires high concentrations[29,35] and uses organic solvents in combination with electric fields,[29,39] which can impede the biofunctionality of the protein.[40,41] Another method to prepare fibrinogen nanofibers is extrusion through alumina nanopores, in which, however, only a low fiber yield was obtained.[42]

To overcome these technical limitations, we have recently introduced salt-induced self-assembly as an efficient approach to prepare dense networks of fibrinogen nanofibers[43] that maintained their unique porous architecture in aqueous buffers.[44] The roughness of nanofibrous fibrinogen was increased by a factor of 15 in comparison to planar or physisorbed fibrinogen and exhibited an undulated micro-topography.[45] Self-assembled fibrinogen nanofibers promoted fibroblast growth up to 72 h in culture and limited *E. coli* infiltration,[45] while enhancing adhesion and spreading of blood platelets.[46] The secondary structure of the nanofibrous scaffolds could be tailored without introducing any pathogenic amyloid transitions,[44] thus avoiding any irreversible conformational changes. Based on these advantages, we now studied the potential of self-assembled fibrinogen nanofibers to serve as scaffolds for skin tissue engineering. Here, we show for the first time that nanofibrous and flat fibrinogen scaffolds support the cocultivation of human dermal fibroblasts and HaCaT keratinocytes for up to 14 days, while preserving the characteristic morphological features and protein expression of both cell types.

## 2. EXPERIMENTAL SECTION

**2.1. Preparation of Fibrinogen Scaffolds for Cell Culture Studies.** Nanofibrous and planar fibrinogen scaffolds were prepared by our previously described salt-induced self-assembly approach.[43,44] Briefly, 100% clottable fibrinogen from human plasma (Merck, Darmstadt, Germany), dissolved in 10 mM $NH_4HCO_3$ (Carl Roth GmbH, Karlsruhe, Germany) in deionized $H_2O$, was dialyzed overnight against the same solution using a cellulose membrane dialysis tube (cutoff 14 kDa; Sigma-Aldrich, Darmstadt, Germany) to obtain a fibrinogen solution. Fifteen millimeter glass coverslips (VWR, Darmstadt, Germany) were cleaned with piranha solution (3:1 of 95% sulfuric acid ($H_2SO_4$)/30% hydrogen peroxide

($H_2O_2$)) before treatment with 5% (3-aminopropyl)-triethoxysilane (APTES, Sigma) in ethanol ($C_2H_5OH$) overnight. Unbound APTES was removed by washing in pure ethanol three times for 5 min, before storing the coverslips dry for further use.

To obtain fibrinogen nanofibers, 5 mg mL$^{-1}$ of the fibrinogen solution was dried in the presence of 2.5× phosphate-buffered saline (PBS, ThermoFisher, pH 7.4) on APTES-modified coverslips. Planar fibrinogen scaffolds were obtained by drying 5 mg mL$^{-1}$ of fibrinogen in 5 mM $NH_4HCO_3$. Drying was performed in a custom-built climate chamber at a relative humidity of 30% and temperature of 24 °C for 12 h.

To maintain the stability of scaffolds in an aqueous environment for further cell culture studies, the scaffolds were cross-linked in formaldehyde (FA) vapor for 2 h after placing them in a sealed beaker. The FA vapor was generated by placing 1 μL of 37% FA solution (Applichem GmbH, Darmstadt, Germany) per cubic centimeter and letting it evaporate in the sealed beaker. After cross-linking and devaporizing for another 30 min, all samples were washed 3 × 15 min with deionized water. We have extensively characterized the nanofibrous topography with dense, porous nanofiber networks of these fibrinogen nanofiber scaffolds as well as the smooth topography of the planar fibrinogen scaffolds previously.[43,45]

To obtain un-cross-linked adsorbed fibrinogen substrates, the so-called physisorbed fibrinogen scaffolds, a slightly modified protocol from a previously published method was used.[46] Fifteen millimeter glass coverslips (VWR) were cleaned with piranha solution (3:1 of 95% sulfuric acid ($H_2SO_4$)/30% hydrogen peroxide ($H_2O_2$)). A 0.1 mg mL$^{-1}$ fibrinogen solution in PBS (Thermo Fisher, pH 7.4) was then dried on the piranha-cleaned coverslips at 4 °C overnight. Subsequently, the scaffolds were washed three times for 5 min with PBS. The physisorbed fibrinogen scaffolds displayed a flat and smooth topography (see Supporting Information, Figure S4), also described earlier.[46]

Nanofibrous, planar, as well as physisorbed fibrinogen scaffolds were placed in wells of nontreated Corning Costar 24-well plates (Sigma) and sterilized for 30 min using the UV light of a laminar flow cabinet (ESI Flufrance) to further use them in cell culture experiments.

**2.2. Cell Culture.** To study the interaction of cells with fibrinogen scaffolds with different topographies, we used normal adult primary human dermal fibroblasts (ATCC PCS-201-012, LGC Standards GmbH, Wesel, Germany) and human HaCaT keratinocytes (CLS Cell Lines Service GmbH, Eppelheim, Germany).

Human dermal fibroblast (HDF) culture was initiated as per the manufacturer's instructions in complete growth medium using Fibroblast Basal Medium (ATCC PCS-201-030), Fibroblast Growth Kit−Low Serum (ATCC PCS-201-041), and 1% (v/v) penicillin/streptomycin in 75 cm$^2$ flasks (Faust Lab Science GmbH) at 37 °C and 5% $CO_2$ in a humidified atmosphere of a cell culture incubator (Heracell 240, ThermoFisher). Next, 80−100% confluent fibroblasts were subsequently cryopreserved in 80% complete growth medium supplemented with 10% FBS (Sigma) and 10% DMSO. Further initiation of cryopreserved cells and subculturing for cell culture experiments was carried out in cell culture medium, i.e., DMEM (Sigma) with 10% FBS and 1% (v/v) penicillin/streptomycin (P/S) in 75 cm$^2$ flasks at 37 °C and 5% $CO_2$.

Cells were subcultured once a week and used for experiments between passage numbers 1 and 10.

HaCaT keratinocytes were maintained in DMEM with 10% FBS and 1% (v/v) P/S in 75 cm$^2$ flasks (Faust Lab Science GmbH) at 37 °C and 5% $CO_2$ in a humidified atmosphere of our cell culture incubator as described earlier.[47] Cells were subcultured once a week and used for experiments between passage numbers 1 and 20.

To perform further viability, morphology, and protein expression studies, cells were seeded on top of sterile fibrinogen scaffolds described earlier, present inside the wells of nontreated Corning Costar 24-well plates (Sigma) at a density of $1 \times 10^4$ cells/cm$^2$ for each cell-type in DMEM with 10% FBS and 1% P/S and incubated for up to 14 days at 37 °C with 5% $CO_2$. For cocultures, the total cell density was kept consistent with monocultures at $1 \times 10^4$ cells/cm$^2$, thus comprising $5 \times 10^3$ cells/cm$^2$ for each cell-type. Cells seeded in TC-treated 24-well plates (Sarstedt, Nürnbrecht, Germany) cultured under the same conditions were used as controls in subsequent biochemical analysis. For Z-stacking analysis of lipophilic membrane dye-labeled cells, $3 \times 10^4$ cells/cm$^2$ for each cell type were used, thus obtaining a total cell density of $6 \times 10^4$ cells/cm$^2$.

**2.3. Cell Viability Analysis.** Cell viability was determined by using the resazurin-based Invitrogen PrestoBlue HS Cell Viability reagent (ThermoFisher), similar to previous studies.[48−50] For this purpose, the PrestoBlue reagent was diluted in a prewarmed (37 °C) cell culture medium at a ratio of 1:10 to obtain a PrestoBlue working solution. Subsequently, medium present at the top of cells present on the fibrinogen scaffolds in 24-well plates was replaced with 200 $\mu$L/well of the PrestoBlue working solution. After 2.5 h of incubation at 37 °C and 5% $CO_2$ under a humidified atmosphere, the supernatant was removed and pipetted into 96-well plates (Sarstedt), and the absorption was measured spectrophotometrically using a Multiskan Sky Microplate Spetrophotometer (ThermoFisher) at 570 nm, using 600 nm as a reference wavelength.

Cell viability was monitored every 3, 7, 10, and 14 days from the same plate. After the supernatant containing PrestoBlue was removed, cells were washed three times with prewarmed (37 °C) PBS. Subsequently, prewarmed (37 °C) cell culture medium (1 mL/well) was added to the plates and returned to the incubator at 37 °C and 5% $CO_2$ before the next measurement.

As a negative control, PrestoBlue working solution was added into empty wells of a 96-well plate (no cells), whereas cells grown in TC-treated plates was treated as the 100% viability control group and both controls treated as described above. To obtain PrestoBlue final absorbance values, first, the absorbance obtained at 600 nm was subtracted from the absorbance at 570 nm for all wells. Then, the mean absorbance of the negative control (containing no cells but media alone) was subtracted from each sample well. To obtain PrestoBlue reduction, the final absorbance values determined from cells grown on fibrinogen scaffolds were normalized to the final absorbance values determined for the 100% viability control.

Specific absorbance

$$= [\text{absorbance at 570 nm}] - [\text{absorbance at reference 600 nm}]$$

$$\text{Final absorbance} = [\text{Specific absorbance of samples}] - [\text{Mean specific absorbance of negative control (no cells)}]$$

$$\text{PrestoBlue reduction (\% of control)} = \frac{\text{Final absorbance}}{\text{Final absorbance of viabiliy control}} \times 100$$

Three independent experiments ($n$ = 3) were performed in triplicate for fibrinogen nanofibers, planar fibrinogen, and physisorbed fibrinogen. Statistical analysis was determined for all viability data using the software Graphpad Prism 8 (GraphPad, San Diego, CA).

**2.4. Cell Morphology Analysis.** To analyze cellular cytoskeletal staining and to visualize overall cell morphology on fibrinogen scaffolds with different topographies, cells were fixated using 4% (v/v) solution of paraformaldehyde (PFA) in PBS (Biotrend, Cologne, Germany) for 30 min at room temperature and were analyzed via fluorescence microscopy as well as SEM imaging.

For cytoskeletal staining, actin filaments of cells grown on fibrinogen scaffolds for 4 days were stained with phalloidin (ActinRed ReadyProbes Reagent, Life Technologies Europe BV, Netherlands) and nuclei were stained with Hoechst H33342 (NucBlue Live ReadyProbes Reagent, Life Technologies) for 30 min at room temperature using 2 drops/500 $\mu$L of PBS. After washing two times with PBS, stained samples were mounted onto glass slides with Prolong Gold antifade mounting medium (ThermoFisher) and cured overnight at room temperature. The specimens were imaged at 40× magnification in an inverted fluorescence microscope (Ti-E − V5.30, Nikon, Tokyo, Japan) and appropriate filter settings ($\lambda_{ex}$ = 540 nm and $\lambda_{em}$ = 565 nm for Actin Red and $\lambda_{ex}$ = 330−380 nm and $\lambda_{em}$ = 435−485 nm for H33342).

Fluorescence images of phalloidin and H33342 stained cells were analyzed using the open-source software ImageJ provided by the NIH,[51] from three independent experiments performed in triplicate for each substrate type, amounting to nine images analyzed per sample. Analysis of the cell orientation was performed using the red and blue channel via the ImageJ plugin OrientationJ and the Origin 2021 software as described earlier.[45,47]

For SEM analysis, cells grown on fibrinogen scaffolds for 10 days were dried with ethanol exchange by gradually increasing the concentration of pure ethanol on the samples. Samples were subsequently sputter-coated with gold for 25 s using a sputter coater 108 auto system (Tescan GmbH, Dortmund, Germany) before SEM imaging with a Zeiss Supra 40 device (Carl Zeiss, Oberkochen, Germany) at an acceleration voltage of 3 kV.

**2.5. Protein Expression.** To analyze protein expression, an immunocytochemical staining was performed on cells growing on top of sterile fibrinogen scaffolds in 24-well plates for 4 days. Staining was conducted for the fibroblast marker protein vimentin[52,53] and the keratinocyte marker protein cytokeratin 14.[52,54] First, cells were fixated using a 4% (v/v) solution of PFA in PBS for 30 min at room temperature. Subsequently, cells were permeabilized with 0.1% (v/v) TritonX-100 (Carl Roth GmbH) in PBS for 10 min at 4 °C followed by incubation with blocking buffer containing 0.3 M glycine (Acròs Organics, Geel, Belgium) and 1% (w/v) BSA
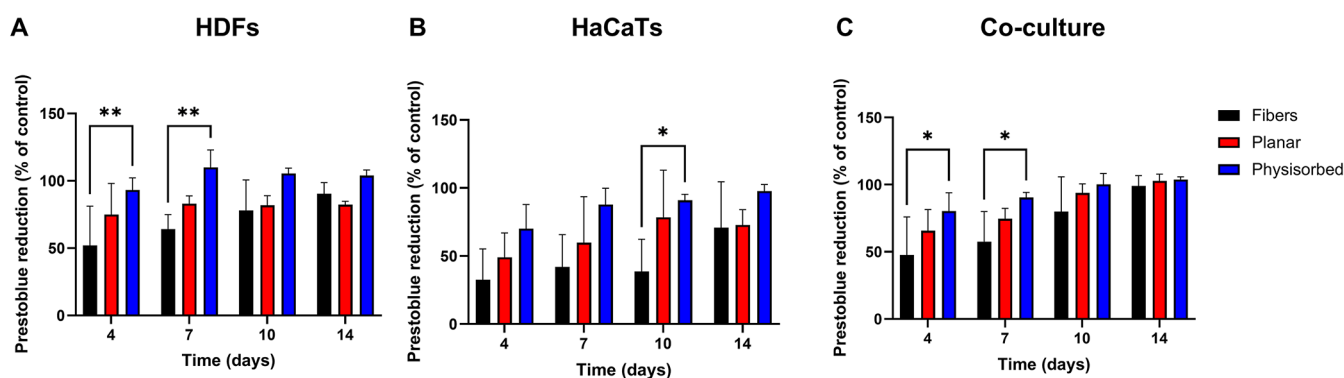
**Figure 1.** Viability of HDFs and HaCaT keratinocytes on fibrinogen with different topographies. 10 000 cells/cm² of HDFs (A) and HaCaTs (B) each or in total for a combination of both cell types in coculture (C) were seeded onto fibrinogen fibers, planar fibrinogen, and physisorbed fibrinogen and cultivated for up to 14 days at 37 °C and 5% CO₂. The cell viability was monitored every 4, 7, 10, and 14 days using the PrestoBlue Cell Viability reagent and is displayed in comparison to cells cultivated on a TC plate as a control. Data shown are presented as means ± standard deviation of values obtained from three independent experiments performed in triplicate. Significant differences were analyzed by two-way ANOVA and are indicated by *$p \leq 0.05$ and **$p \leq 0.01$. Very similar cell viabilities were observed on the different fibrinogen topographies with the cocultures showing values closer to 100% of the control compared to the individual monocultures. The highest overall increase in PrestoBlue reduction rate was observed for cells on nanofibers, whereas cells grown on physisorbed Fg showed the highest overall viability.

(Sigma) in PBS to block unspecific antibody binding. After washing three times with PBS, samples were incubated overnight at 4 °C with 40 μL of a diluted primary antibody solution, inverted on parafilm under a humidified atmosphere. Either a combination of the primary antibodies Invitrogen monoclonal anti-Vimentin antibody (SP20; ThermoFisher) and Invitrogen monoclonal anti-Cytokeratin 14 antibody (LL002; ThermoFisher) in a dilution of 1:200 and 1:100 respectively in 1% (w/v) BSA in PBS or only the polyclonal anti-Fibronectin primary antibody (Sigma) in a dilution of 1:400 in 0.1% (w/v) BSA in PBS was applied. Samples were washed three times with PBS before incubation with secondary antibodies at 4 °C for 1 h in the dark at a dilution of 1:1000 in 1% (w/v) BSA. Secondary antibodies utilized were Atto 647N polyclonal goat antirabbit IgG (Sigma) and Alexa Fluor 488 polyclonal donkey antimouse IgG (ThermoFisher). After washing two times with PBS, stained samples were mounted onto glass slides with Prolong Diamond antifade medium with DAPI and cured overnight at room temperature. All samples were imaged at 40× magnification in our inverted Nikon fluorescence microscope with appropriate filter settings ($\lambda_{ex}$ = 647 nm and $\lambda_{em}$ = 665 nm for Atto 647 violet, $\lambda_{ex}$ = 488 nm and $\lambda_{em}$ = 520 nm for Alexa 488 green, and $\lambda_{ex}$ = 330−380 nm and $\lambda_{em}$ = 435−485 nm for DAPI blue).

**2.6. Cell Labeling with Lipophilic Membrane Dyes.** To distinguish between both cell types on a fibrinogen scaffold in the coculture setup, they were labeled with lipophilic cell membrane dyes before seeding. HDFs were labeled with Invitrogen Vybrant DiI Cell-Labeling Solution (Thermo-Fisher), and HaCaTs were labeled with Invitrogen Vybrant DiO Cell-Labeling Solution (ThermoFisher). Following trypsination, cells were centrifuged, and the cell pellet was subsequently resuspended in prewarmed (37 °C) serum-free cell culture medium DMEM, before diluting the suspensions to a cell density of 60 000 cells/mL. These cells were incubated with 5 μL of the respective cell labeling solution per milliliter of cell suspension for 15 min at 37 °C in the dark. The labeled cell suspensions were centrifuged at 1500 rpm for 5 min, the aspirated supernatant and cell pellet were then gently resuspended in prewarmed (37 °C) cell culture medium DMEM with 10% FBS. These centrifugation and resuspension

steps were repeated two more times before the labeled cells were seeded onto the scaffolds at a density of 30 000 cells/cm².

To obtain a layered skin construct, DiI-HDFs (red) were seeded onto the scaffolds using the above-described procedure and cultivated at 37 °C and 5% CO₂ for 3 days before the seeding of DiO-HaCaTs (green) by the same procedure on top of HDFs. Six days after the seeding of HaCaTs, cells on the scaffolds were fixated with a 2% (v/v) solution of PFA in PBS for 30 min at room temperature. All samples were subsequently mounted onto glass slides with Prolong Diamond antifade medium with DAPI and cured overnight at room temperature. Stained cells on fibrinogen scaffolds were imaged using z-stacking at 60× magnification in our inverted fluorescence microscope with appropriate filter settings ($\lambda_{ex}$ = 540 nm and $\lambda_{em}$ = 565 nm for DiI orange-red, $\lambda_{ex}$ = 488 nm and $\lambda_{em}$ = 520 nm for DiO green, and $\lambda_{ex}$ = 330−380 nm and $\lambda_{em}$ = 435−485 nm for DAPI blue). For z-stack analysis, we recorded 10 to 12 images over a total z-height of up to 6 μm with a step size of 500 nm.

## 3. RESULTS

**3.1. Viability of HDFs and HaCaTs on Self-Assembled Fibrinogen Scaffolds.** Using a PrestoBlue assay, comparable cell viabilities for HDF or HaCaT monocultures and cocultures were obtained on nanofibrous, planar, as well as physisorbed fibrinogen scaffolds up to 14 days (see Figure 1). Overall better cell viability values as well as an increase in the cell metabolism rate indicated by an increase in PrestoBlue reduction were observed for cells grown at a cell density of 10 000 cells/cm² on these substrates (see Figure 1) compared to a lower initial cell seeding density of 5000 cells/cm² (see Supporting Information, Figure S1). In particular, much lower PrestoBlue reduction values were observed for cells on fibrinogen fibers in comparison to planar and physisorbed fibrinogen at this lower cell density (c.f. Figure S1 and Figure 1), indicating the requirement of an initial critical cell number for a robust adhesion and growth of both cell types on fibrinogen nanofibers.

Cells on physisorbed fibrinogen scaffolds showed an overall PrestoBlue reduction closest to 100% of the control, i.e., viability of cells on TC-treated plates (see Figure 1A, B, and
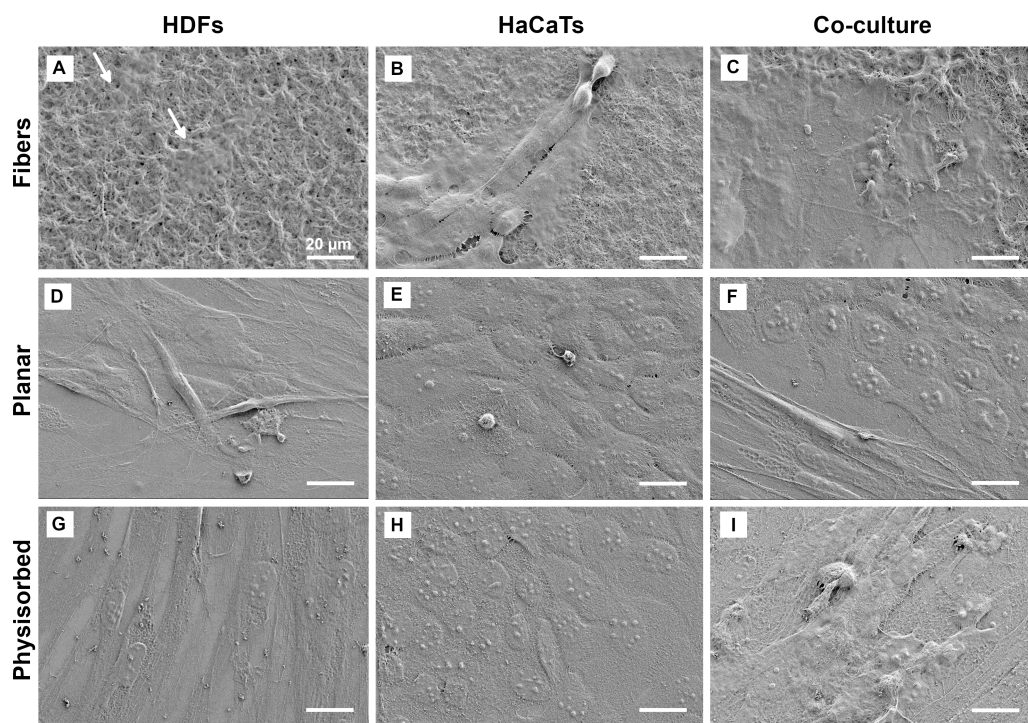
**Figure 2.** SEM images of HDFs and HaCaTs grown on fibrinogen scaffolds with different topographies. HDF and HaCaT monocultures or a combination of both cell types (coculture) were seeded onto fibrinogen with nanofibrous topography (A–C), planar topography (D,E), or physisorbed fibrinogen (G–I), and SEM analysis was performed after 10 days of cultivation. Very distinctive cell morphologies were observed for both monocultures on the different fibrinogen topographies, with flat and elongated cell bodies for HDFs and clustered and roundish cell bodies for HaCaTs. These morphological features were unchanged on all fibrinogen substrates when both cell types were grown in coculture. Scale bar of 20 $\mu$m represented in panel A applies to all other panels, B–I.

C). For cells on physisorbed fibrinogen, we also observed a higher overall cell metabolism compared to cells on nanofibrous and planar fibrinogen scaffolds. HDF monocultures on physisorbed fibrinogen already showed a high initial PrestoBlue reduction around 100% and remained stable until the end of the incubation period (see Figure 1A). The PrestoBlue reduction of HaCaT monocultures on physisorbed fibrinogen increased from 70% on day 4 to 98% of control on day 14, respectively (see Figure 1B). Similar was the case for cocultures on physisorbed fibrinogen where PrestoBlue reduction was significantly higher on day 10 and day 14 amounting to about 100% of the control for both days, compared to 80% of the control on day 4 (see Figure 1C).

In general, PrestoBlue reduction of HaCaT monocultures on nanofibrous and planar fibrinogen scaffolds was lower than for HDF monocultures and cocultures (c.f. Figure 1A, B, and C). Moreover, cocultures showed the highest increase in cell metabolic activity over time on these scaffolds, with an increase in PrestoBlue reduction from 48% on day 4 to 99% on day 14 on fibrinogen fibers and 66% on day 4 to 103% of control on day 14 on planar fibrinogen (see Figure 1C). Although cell metabolic activities of monocultures on fibers and planar fibrinogen (see Figure 1A, B) did not differ from the cocultures (see Figure 1C) for up to 7 days, a higher PrestoBlue reduction of cocultures in comparison to the respective monocultures was evident latest by the end of 10 days of cultivation. The cell metabolic activity of HDFs and cocultures on fibrinogen fibers differed significantly from that for the cells grown on physisorbed fibrinogen at the initial stage up to 7 days but leveled out to around 100% of the control at the end of 14 days (c.f. Figure 1A and C).

On the whole, all three fibrinogen topographies yielded a robust overall cell viability and proliferation of HDF or HaCaT monocultures as well as cocultures and were therefore considered highly biocompatible for both cell types.

**3.2. Morphology of HDFs and HaCaTs upon Interaction with Fibrinogen Scaffolds.** SEM analysis of HDF and HaCaT mono- and cocultures on different fibrinogen topographies after 10 days revealed slightly lower cell densities on fibrinogen nanofibers, compared to planar or physisorbed fibrinogen (see Figure 2). A very flat overall cell morphology was observed on nanofibrous fibrinogen scaffolds for HDFs. Individual HDF cells were difficult to distinguish from the underlying fibers in monocultures (see Figure 2A) and cocultures (see Figure 2C). HaCaTs on nanofibrous fibrinogen fibers also adhered closely to the fibers but were more visible due to their elevated cell bodies when cultivated in monoculture (see Figure 2B) but hard to distinguish based on their morphology, similar to the HDFs (see Figure 2C). On the other hand, HDFs showed a very distinct elongated, spindle-shaped morphology on planar fibrinogen (see Figure 2D) and physisorbed fibrinogen (see Figure 2G), whereas HaCaTs appeared polygonal with many short filopodia and clustered on both flat substrates (see Figure 2E and H). For cocultures on nanofibrous and physisorbed fibrinogen, we found areas where both cells had grown in layers (see Figure 2C and I). In contrast, on planar fibrinogen, HDFs and HaCaTs had grown next to each other and could be well distinguished based on their distinct cell morphologies (see Figure 2F).

Subsequently, fluorescence microscopy of phalloidin-stained actin filaments (see Figure 3) revealed that the morphological
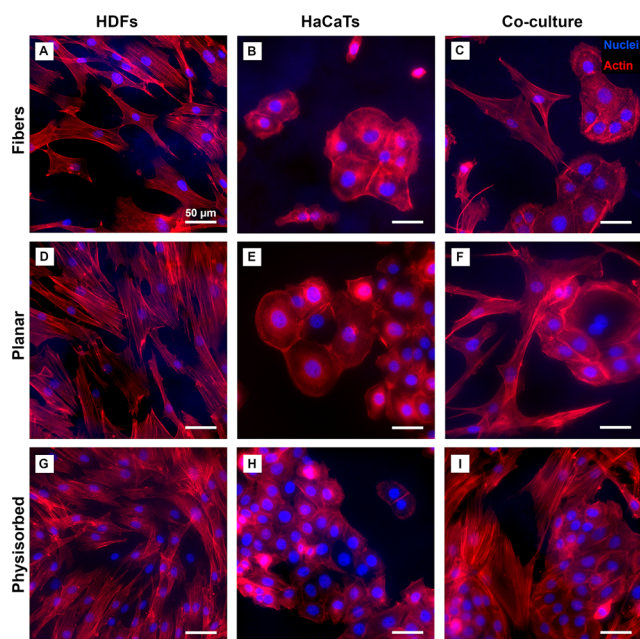
**Figure 3.** Cytoskeletal staining of HDFs and HaCaTs on different fibrinogen topographies. HDF and HaCaT monocultures or a combination of both cell types (coculture) were seeded onto nanofibrous fibrinogen (A−C), planar fibrinogen (D−F), and physisorbed fibrinogen (G−I) and stained for their actin cytoskeleton (red) with phalloidin and nuclei (blue) with H33342 after 4 days of cultivation. The contrasting cell morphologies for the two cell types on all fibrinogen topographies were evident with elongated HDFs and clustered and polygonal HaCaT cells. In the coculture model, the two cell types were observed growing adjacent to each other and could be easily distinguished based on their morphology alone. Scale bar of 50 μm represented in panel A applies to all other panels B−I.

S3), suggesting a random cellular alignment based on their actin cytoskeleton. Overall, the native cell morphology and cytoskeletal orientation of both cell types in coculture remained unchanged despite the differences in topography of the underlying fibrinogen scaffolds.

**3.3. Immunocytochemical Characterization of HDFs and HaCaTs on Fibrinogen Scaffolds.** When analyzing the expression of selected marker proteins by immunocytochemistry after 4 days, HDF monocultures stained positive for the mesenchymal marker protein vimentin, and HaCaTs monocultures were positive for the keratinocyte marker cytokeratin 14 (see Figure 4). Under these conditions, no counter staining
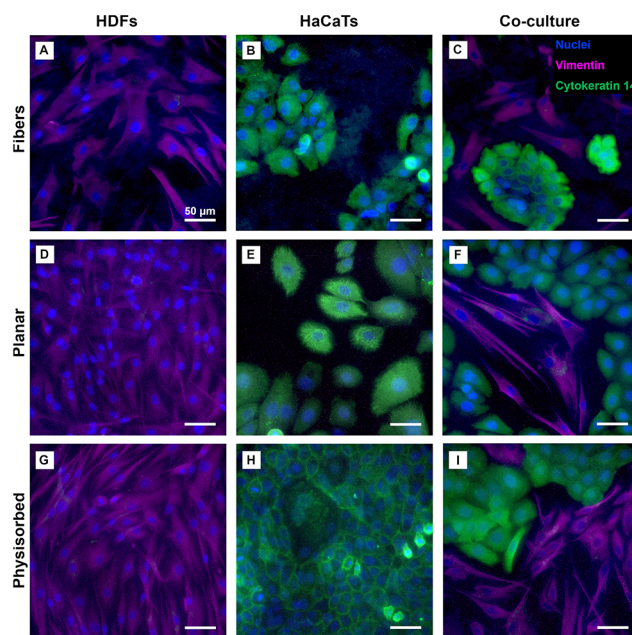


**Figure 4.** Immunocytochemical staining for cell-specific markers of HDFs and HaCaTs on different fibrinogen topographies. HDF and HaCaT monocultures or a combination of both cell types (coculture) were seeded onto fibrinogen scaffolds with different topographies, and an immunocytochemical staining was performed after 4 days of cultivation. HDFs were observed to be positive for the mesenchymal marker protein vimentin (purple), whereas HaCaTs were positive for the keratinocyte marker protein cytokeratin 14 (green) on nanofibrous (A−C), planar (D−F), and physisorbed (G−I) fibrinogen. All cells were additionally stained with DAPI to visualize cell nuclei (blue). In the coculture model, both cell types were growing adjacent to each other and could be distinguished by the expression of the respective cell-specific protein markers. Scale bar of 50 μm represented in panel A applies to all other panels B−I.

differences between HDFs and HaCaTs on all three fibrinogen topographies were consistent with those observed by SEM as well as with cells cultivated on TC-treated plates (see Supporting Information, Figure S2A−C). On the different fibrinogen topographies, HDF monocultures exhibited a typical fibroblast morphology, and elongated cells with defined, linear actin filaments were observed (see Figure 3A, D, and G). This was in contrast to polygonal HaCaTs, which were present in clusters on all three fibrinogen topographies and shown to have a more diffusive actin cytoskeleton (see Figure 3B, E, and H). For cocultures on different fibrinogen topographies, individual HDFs and HaCaTs were found growing next to each other and could be easily distinguished by their cytoskeletal staining and, in turn, their morphology (see Figure 3C, F, and I).

Moreover, the slightly lower cell density on fiber scaffolds compared to planar and physisorbed fibrinogen agreed well with our SEM analysis. However, for both monocultures and the coculture setup, the lower cell number correlated with larger cell sizes on nanofibrous (see Figure 3A−C) and planar fibrinogen (see Figure 3D−F) compared to the respective cells cultivated on physisorbed fibrinogen (c.f. Figure 3G−I) as well as on TC-treated plates (see Figure S2A−C). Furthermore, when we analyzed the cytoskeletal orientation of HDFs and HaCaT monocultures and cocultures, we observed that no preferential orientation was prevalent on any of the fibrinogen scaffolds despite the strong topographical differences between fibrous and flat substrates (see Supporting Information, Figure

of vimentin for HaCaTs or cytokeratin 14 staining for HDFs grown on any of the three fibrinogen scaffolds was observed. Expression of the respective marker proteins was found to be independent of the underlying fibrinogen topography. As already observed from SEM analysis and cytoskeletal staining, an overall slightly lower cell density was observed on fibrinogen nanofibers (see Figure 4A−C), compared to cells cultivated on both flat fibrinogen topographies (see Figure 4D−I).

The cell type-specific protein expression was maintained under the condition where HDFs and HaCaTs were grown in coculture on all fibrinogen scaffolds (see Figure 4C, F, I). Consequently, both cell types grown on nanofibrous (see Figure 4C), planar (see Figure 4F), and physisorbed (see

Figure 4I) fibrinogen could be distinguished, and individual cells could be detected solely based on their cell-type-specific protein expression. This characteristic expression of marker proteins was consistent with a positive control of cells cultivated in monoculture or coculture on TC-treated plates (see Supporting Information, Figure S2D−F). Therefore, both HDFs and HaCaTs maintained their basal phenotype when cultivated in monoculture and coculture on fibrinogen fibers as well as on planar and physisorbed fibrinogen as confirmed from their positive native protein expression.

**3.4. Deposition of ECM Protein Fibronectin on Fibrinogen Scaffolds.** To assess whether HDFs and HaCaTs grown on fibrinogen scaffolds with different topographies support a buildup of a new ECM, we exemplarily studied the expression of fibronectin, an important ECM protein that is considered vital in the process of wound healing.[55] For this, we performed a fibronectin immunostaining, and counter nuclei staining with DAPI was performed after 4 days of cultivation (see Figure 5). HDF monocultures on fibrinogen fibers (see
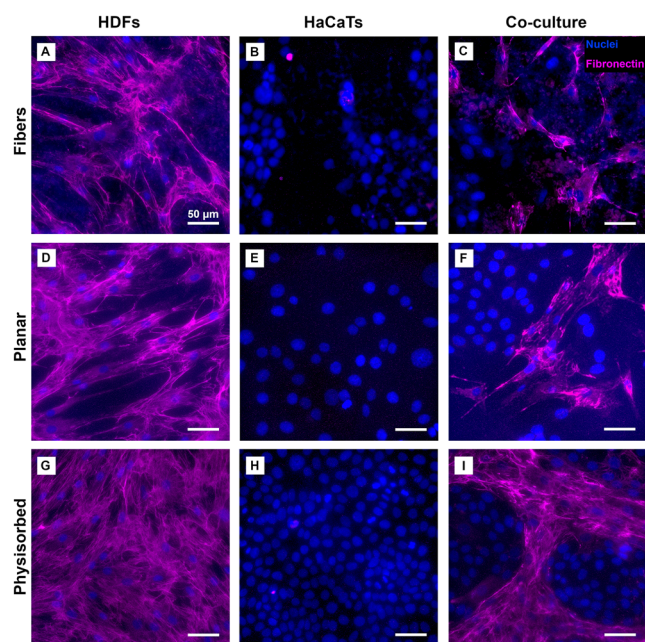


**Figure 5.** Staining for fibronectin after growth of HDFs and HaCaTs on different fibrinogen topographies. HDF and HaCaT monocultures or a combination of both cell types (coculture) were seeded onto nanofibrous (A−C), planar (D−F), and physisorbed (G−I) fibrinogen and an immunocytochemical staining for fibronectin (purple) was performed after 4 days of cultivation. HDFs were observed to be positive for the ECM marker protein, whereas HaCaTs did not show any fibronectin expression on any of the fibrinogen substrates. In HDF monocultures, the staining seemed to not only be confined to the cell bodies but was more widespread and distributed beyond the margins of the cell bodies as individual HDFs were difficult to distinguish. All cells were additionally stained with DAPI to visualize cell nuclei (blue). Scale bar of 50 μm represented in panel A applies to all other panels B−I.

Figure 5A), on planar (see Figure 5D), and on physisorbed fibrinogen (see Figure 5G) were positive for the expression of the ECM marker fibronectin. In contrast, HaCaT mono-cultures did not express any fibronectin irrespective of the fibrinogen substrate on which they had been cultivated (see Figure 5B, E, and H). Similarly, when both cell types were

grown in a coculture setup, the fibronectin staining seemed to be limited to the area where HDFs were present, since HaCaT clusters, which were visible via their nuclei, showed an absence of fibronectin staining. This was the case when cocultures were cultivated on nanofibrous (see Figure 5C), planar (see Figure 5F), and physisorbed fibrinogen (see Figure 5I), which agreed with such a staining performed on cells cultivated on TC-treated plates as a positive control (see Supporting Information, Figure S2G−I). A slightly lower overall cell density on fibrinogen nanofibers, compared to cells cultivated on the other two fibrinogen substrates, was consistent with that observed from previous microscopic analyses. In this case, the fibronectin expression appeared to be proportional to the cell density. Thus, HDFs cultivated on fibrinogen nanofibers in monoculture or in coculture with HaCaTs seemed to maintain their characteristic phenotype of fibronectin secretion, as was the case for HDFs cultivated on planar and physisorbed fibrinogen.

**3.5. Fibrinogen Scaffolds with HDFS and HaCaTs as Multilayered Constructs.** To better distinguish between HDFs and HaCaTs that were successively seeded on top of fibrinogen scaffolds, cells were labeled with different fluorescent lipophilic dyes prior to seeding. A 3-day pregrowth period for HDFs was ensured before seeding of HaCaTs and further investigation via z-stacking after 6 days (see Figure 6).
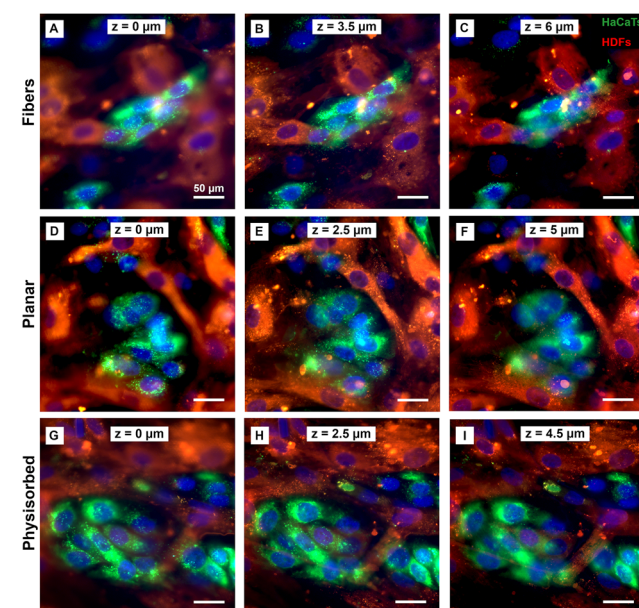


**Figure 6.** Z-stack images of layered cocultures of HDFs and HaCaTs labeled with lipophilic membrane dyes on different fibrinogen topographies. HDFs stained with DiI (red) were seeded onto nanofibrous (A−C), planar (D−F), and physisorbed (G−I) fibrinogen followed by a seeding of DiO-stained HaCaTs (green) after 3 days. After a total of 6 days of cultivation, 10−12 z-stack images were taken with a step size each of 500 nm and a total thickness of 6 μm on fibrinogen nanofibers, 5 μm on planar fibrinogen and 4.5 μm on physisorbed fibrinogen. All cells were additionally stained with DAPI to visualize cell nuclei (blue). Scale bar of 50 μm represented in panel A applies to all other panels B−I. HaCaTs (green) were observed to be in focus on the top (A, D, G). Both cell types were in focus in the middle layers (B, E, H), whereas HDFs (red) were in focus at the bottom (C, F, I), thus indicating a layering of both cell types on all fibrinogen topographies.

HaCaTs were seen growing at the topmost layer on fibrinogen nanofibers (see Figure 6A) and planar (see Figure 6D) and physisorbed fibrinogen (see Figure 6G), indicated by cells in the top focal plane possessing a green signal from the DiO labeling. This was accompanied by red background fluorescence signals from HDFs, which were not in focus. Fluorescence signals which could be attributed to both cell types, green for DiO-labeled HaCaTs and red for DiI-labeled HDFs, were found in focus in the middle cell layers on all fibrinogen topographies (see Figure 6B, E, and H). The nanofibrous fibrinogen construct appeared to have the maximum thickness with HDFs growing on the bottom layer with a total z-height of 6 $\mu$m, indicated by cells possessing a red signal in the lowest focal plane (see Figure 6C). Similar red fluorescence signals were observed in focus for planar fibrinogen (see Figure 6F) with a slightly lesser total z-height of 5 $\mu$m followed by physisorbed fibrinogen with a z-height of 4.5 $\mu$m (see Figure 6I), indicating the presence of HDFs. Thus, although completely confluent bilayers of HDFs and HaCaTs were not observed after 6 days of cultivation, the successive stacking of cells on top of all fibrinogen topographies was successful.

To achieve a multilayered construct with confluent cell layers, HDFs and HaCaTs were successively seeded on top of fibrinogen scaffolds for 14 days of cultivation, which included a 4-day pregrowth period for HDFs before the seeding of HaCaTs. Cell viability analysis of this setup revealed significant differences in cell metabolic activity at the end of day 4 for HDFs alone cultivated on nanofibrous, planar, or physisorbed fibrinogen (see Figure 7A). However, on subsequent days, comparable and constantly high cell metabolic activities were observed, after HaCaTs were seeded on top of HDFs. Layered cocultures showed overall PrestoBlue reduction close to 100% of the control, i.e., cells grown on TC-treated plates, up to 14 days after cultivation, thus indicating a robust cell viability on all fibrinogen topographies.

SEM analysis of these layered cocultures after 14 days of cultivation showed a confluent layer of polygonal HaCaTs with many short filopodia on all fibrinogen topographies and the absence of a distinct elongated and spindle-shaped morphology of HDFs (see Figure 7B−D). This was in concurrence with cell morphology observed in HaCaT monocultures on flat substrates (c.f. Figure 2E and H). Moreover, small gaps between cells in the top HaCaT layer revealed that the cells were indeed present in multiple layers on all fibrinogen topographies. Thus, a multilayered cell-biomaterial construct with HaCaTs in the topmost layer and HDFs below was achieved on all fibrinogen topographies.

## 4. DISCUSSION

In this study, we showed for the first time that self-assembled fibrinogen nanofibers support the cocultivation of human dermal fibroblasts and HaCaT keratinocytes as well as planar and physisorbed fibrinogen. This finding demonstrates the potential of nanofibrous fibrinogen as a novel scaffold material for skin tissue engineering, in particular when both cells are cultivated successively to form multilayers.

**Nanofibrous and Flat Fibrinogen Topographies Support Cell Adhesion and Long-Term Viability.** Cell adhesion of HDFs and HaCaTs was supported by nanofibrous, planar, and physisorbed fibrinogen scaffolds promoting cell growth up to 14 days with viabilities reaching 100% in comparison to TC-treated plates, for both mono- and
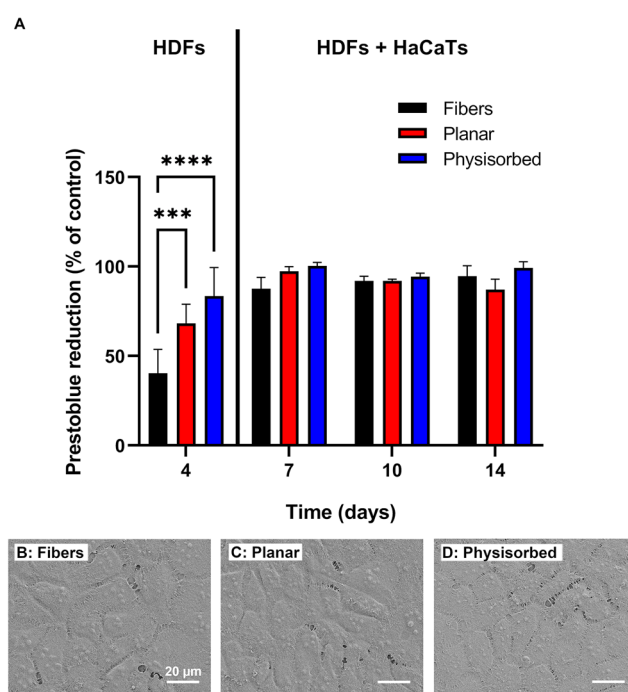


**Figure 7.** Viability analysis and SEM images of layered cocultures of HDFs and HaCaT keratinocytes on fibrinogen with different topographies. 10 000 cells/cm$^2$ of HDFs were seeded onto fibrinogen fibers, planar fibrinogen, and physisorbed fibrinogen followed by 10 000 cells/cm$^2$. HaCaTs at the end of day 4 and cultivated for up to 14 days at 37 °C and 5% CO$_2$ to obtain a layered coculture. The cell viability was monitored every 4, 7, 10, and 14 days using the PrestoBlue Cell Viability reagent and is displayed in comparison to cells cultivated on a TC plate as the control (A). Data shown are presented as means ± standard deviation of values obtained from three independent experiments performed in triplicate. Significant differences were analyzed by two-way ANOVA and are indicated by ***$p \leq 0.001$ and ****$p \leq 0.0001$. SEM analysis was performed after 14 days of layered cocultivation on fibrinogen with nanofibrous topography (B), planar topography (C), or physisorbed fibrinogen (D). After seeding of HaCaTs in the layered coculture, very similar cell viabilities were found on the different fibrinogen topographies between days 7 and 14, and after 14 days only polygonal HaCaTs with many short filopodia were observed on all fibrinogen topographies via SEM.

cocultures (see Figure 1). This result agrees well with previous studies of fibroblast/keratinocyte cocultures on fibrin, collagen, or polystyrene constructs that were conducted between 5 and 22 days.[25,26,56−59] Comparing the different fibrinogen topographies, the cell metabolic activity increased the most on fibrinogen fibers, both for mono- and cocultures, followed by planar and physisorbed fibrinogen, where higher cellular metabolic activities were already observed early on, indicating a robust cell viability. We assume that the lower initial values in cellular metabolic activity, which might correspond to the observed lower cell numbers on fibrinogen fibers at an earlier time point, are attributed to the 15-fold higher surface roughness and undulated microtopography of the nanofiber scaffolds[43,45] in comparison to planar or physisorbed fibrinogen. Therefore, the cells presumably required more time to adhere to the fibers and form a confluent layer than on the flat topographies as we had previously observed with blood platelets, which showed cell spreading exclusively on fibrinogen nanofibers, whereas round platelets were observed on planar

and physisorbed fibrinogen.[46] On the other hand, due to their high surface-to-volume ratio, the 3D network of fibrinogen nanofibers offers more binding sites for HDFs and HaCaTs than planar or physisorbed fibrinogen.[46] This high ligand density might be responsible for the observed strong increase in cell metabolic activity on fibrinogen nanofibers over time. Interestingly, we observed no significant differences in cell viability or morphology when HDFs and HaCaTs were grown on cross-linked nanofibrous and planar fibrinogen, compared with uncross-linked physisorbed fibrinogen. A previous study reported that glutaraldehyde cross-linking of fibrinogen-PCL nanofibers significantly reduced the proliferation of keratinocytes already after 7 days,[39] which was however not the case for FA vapor treatment even after 14 days in this study. Instead, for nanofibrous and planar fibrinogen (both cross-linked) and for uncross-linked physisorbed fibrinogen, no significant differences in cell viability were found after 14 days in all cell culture setups. We therefore conclude that the cross-linking procedure did not affect the cell viability, which is in good agreement with our previous study on 3T3 fibroblasts.[45]

When we cocultivated HDFs and HaCaT keratinocytes as model system for skin cells, both cell types were maintained in standard DMEM-FBS cell culture medium, consistent with coculture models of these cell types in 3D fibrin gels,[25] on collagen microfiber scaffolds,[60] in 3D collagen-fibrin constructs,[56] and in fibrin-PLLA-collagen hydrogels.[61] While fibroblasts are known to adhere to the Arg–Gly–Asp (RGD) sequence of fibrin(ogen) via $\alpha_V\beta_3$ integrins,[20,62] keratinocytes are not expected to adhere to fibrin(ogen), since they do not express $\alpha_V\beta_3$ integrins.[63] Even so, similar to our findings, other studies have reported adhesion and proliferation of keratinocytes in 3D fibrin constructs,[26] fibrin gels,[64] fibrin-alginate sponge scaffolds,[65] and PCL-fibrin constructs.[66] Previously, laminin-binding protein (LB69)-mediated attachment of keratinocytes to fibrinogen-coated dishes as well as fibrin,[67] or epidermal growth factor (EGF) receptor-mediated adhesion of keratinocytes to fibrin gel layers[64] has been suggested. Such nonintegrin mediated binding strategies might be responsible for HaCaT keratinocyte adhesion to different fibrinogen topographies in this study. Additionally, previously reported fibrin-mediated disruption of adhesion of differentiated keratinocytes, but not of undifferentiated keratinocytes,[68] underlines the good adhesion of undifferentiated HaCaT keratinocytes to all fibrinogen scaffolds observed in this study.

Secretion of several cytokines, chemokines, and growth factors has been identified in keratinocyte–fibroblast interactions during wound healing[69] as well as in autologous skin substitutes.[70] Some vital interactions include keratinocyte stimulation of fibroblasts to induce keratinocyte growth factor (KGF) through the production of interleukin-1, which in turn modulates keratinocyte proliferation and differentiation[12,71] as well as secretion of transforming growth factor (TGF)-$\beta$ by both cell types, which regulates differentiation of fibroblasts.[69,71] The higher cellular metabolic activities of cocultures on fibers and planar fibrinogen at a later time of cultivation in comparison to the respective monocultures in this study (see Figure 1) indicates that the presence of both cell types together over longer periods benefits their growth, in turn signifying a cross-talk between both cells.[12] This might suggest an exchange of growth factors between the two cell types consistent with a previous report of such a coseeding within 3D fibrin gels.[26] Similar cross-talk has also been reported for

cell proliferation within polystyrene scaffolds,[59] in collagen and fibrin constructs with PLA nanofibers,[58] and for cell migration in 3D fibrin gels.[25] Based on the good long-term viability of human dermal fibroblasts and keratinocytes in our coculture model, we conclude that all fibrinogen topographies were highly biocompatible, and we suggest that cell growth was supported by a cross-talk between both cell types, which will be highly interesting to further explore using cytokine detection studies.

**Fibroblasts and Keratinocytes Maintain Their Cell Type-Specific Morphology on Fibrinogen Scaffolds.** SEM analysis in this study showed for the first time that fibrinogen fibers including their distinctive interconnected network architecture remained intact at least for 10 days (see Figure 2), which exceeds our previous cultivation time by 7 days.[45] Overall, the characteristic morphology of the different fibrinogen scaffolds was not altered by the different cell cultures, as shown by comparison with scaffolds without cells presented in our previous studies.[45,46] SEM analysis and cytoskeletal staining further revealed that the native morphology of both fibroblasts and keratinocytes[72–74] was preserved on fibrinogen nanofibers and was unchanged in comparison to cultivation on planar and physisorbed fibrinogen, which is consistent with findings reported for fibrous PLC,[75] 3D fibrin gels,[25] and porous collagen–chitosan scaffolds.[76] Both cell types appeared very flat on the different fibrinogen topographies, indicating very good cell adhesion. Overall, cell type-dependent differences in cell morphology were more evident on planar and physisorbed fibrinogen than on fibrinogen nanofibers, which may be due to cells aligning with the undulated fiber topography.

Cytoskeletal staining further revealed defined, linear actin filaments in the elongated fibroblasts on all fibrinogen topographies, whereas a more diffusive actin cytoskeleton in the polygonal keratinocytes was consistent with a previous study using fibrinogen-sodium alginate sponge scaffolds[65] (see Figure 3). Thus, there appeared to be a cell type-dependent difference in actin cytoskeleton, which was independent of the underlying fibrinogen substrate. Interestingly, this observation contrasts with our previous findings where mouse 3T3 fibroblasts showed topography-dependent cytoskeletal changes with more pronounced actin stress fibers on planar fibrinogen than on nanofibers.[45] We assume that the observed differences in the actin cytoskeleton can mainly be attributed to the different fibroblast type and longer cultivation times used in this study.

Differences in actin cytoskeletal organization can not only be governed by intrinsic cellular morphogenetic potentials of fibroblasts and keratinocytes but also by differences in available extracellular adhesions.[73] The rather diffused actin cytoskeleton of HaCaT keratinocytes on all fibrinogen topographies in this study might be attributed to nonintegrin mediated cell adhesion mechanisms, as we have also previously observed for these cells on other substrates.[47] Thus, not only intrinsic morphological characteristics but also different cell adhesion mechanisms might explain the differences in actin cytoskeletal organization between the two cell types that appeared on the different fibrinogen topographies.

**Expression of Cell-Specific Markers and Fibronectin Deposition Are Promoted by Fibrinogen Scaffolds.** When analyzing the expression of characteristic marker proteins of HDFs and HaCaTs, native protein expression was maintained for cells grown on all fibrinogen topographies

either in monoculture or in coculture (see Figure 4). Hence, we conclude that both cell types preserved their basal phenotype, that is, fibroblast expression of mesenchymal marker vimentin and keratinocyte expression of cytokeratin 14, which is very consistent with other studies reporting on polymer scaffolds,[52] fibrillar collagen films,[53] porous polystyrene scaffolds,[77] and collagen-containing 3D skin organoids.[78]

Vimentin, also known as a fibroblast intermediate filament, serves as a measure of internal quality control, and the absence of such a staining in fibroblasts often indicates significant damage to tissue antigens and the loss of structural architecture.[79] Alternatively, expression of cytokeratin 14 is largely restricted to the epidermal basal skin layer physiologically, thus indicating an undifferentiated HaCaT phenotype,[54,77] as observed in this study. Previously, fibrin layers have been reported to selectively disrupt the adhesion of differentiated keratinocytes, which could be prevented by the addition of calcium to the cell culture medium.[68] Although HaCaTs usually remain in the basal undifferentiated state when maintained at a low calcium concentration, they have been reported to maintain this basal phenotype when cultured continuously at a high calcium concentration and/or when present at less than 80% confluence,[54] as was the case in our study. This supports our observation of HaCaT keratinocyte adhesion to the different fibrinogen substrates as well as their undifferentiated phenotype detected in this study, cultivated in standard DMEM cell culture medium containing a high calcium concentration (1.8 mM).[80]

During the process of normal wound healing, fibroblasts are known to deposit a cellular fibronectin-rich ECM.[81] We observed that the secretion of fibronectin by HDFs, indicative of buildup of new ECM, was unchanged on fibrinogen nanofibers compared to planar and physisorbed fibrinogen in contrast to HaCaTs, which were fibronectin-negative on all fibrinogen topographies as expected (see Figure 5). A distinctive fibronectin expression was also detected when HDFs were cocultured with HaCaT keratinocytes, consistent with an earlier study exploring the reconstruction of human skin cultivated in a 3D nylon mesh[82] or recent reports using inert polystyrene scaffolds[77] as well as the generation of human skin organoids where stem cells differentiated into fibroblasts and keratinocytes.[78] Overall, our findings indicate the presence of a provisional regenerative ECM-secreting fibroblast phenotype, as described earlier,[52,83,84] which will be highly beneficial to exploring our fibrinogen scaffolds further for skin tissue engineering and wound healing therapy.

**Fibrinogen Scaffolds Support a Successive Bilayered Coculture of Fibroblasts and Keratinocytes.** To better mimic the native epidermal–dermal structure, fibrinogen scaffolds were explored for a successive multilayered coculture of HDFs and HaCaT keratinocytes as previously used to study the interaction of both cell types with other scaffold materials, such as collagen hydrogels[56] or 3D sericin constructs.[85] Z-stack analysis of fluorescently labeled HDFs and HaCaTs indicated that a sequential growth of both cell types on all fibrinogen topographies was successful after 6 days of cultivation (see Figure 6). The absence of completely confluent bilayers of fluorescently labeled HDFs and HaCaTs could be attributed to the lower period of cultivation in comparison with the constructs previously analyzed via SEM (c.f. Figure 2). Nevertheless, no longer was cultivation of prelabeled cells possible since longer cultivation times hindered the uniform

distribution of the dyes among the cell population (data not shown). This technical limitation was also reported previously for fluorescent dye-labeled cells in 3D fibrin gels.[25] Similarly to our study, control over local cell seeding density, cellular spatial arrangement, and measurement of cellular responses in layered cocultures of prelabeled fibroblasts and keratinocytes have also been reported previously in 3D collagen constructs with fibrin beads.[56]

Therefore, to further study bilayered confluent cocultures after 14 days of cultivation, we performed cell viability and SEM analysis (see Figure 7). Cell viability of the biomimetic layered coculture was very well supported on all fibrinogen topographies for 14 days as indicated by consistently high cell metabolic activities. SEM analysis after 14 days of culture revealed the presence of a confluent layer of HaCaT keratinocytes on top of other cells, strongly suggesting a successful multilayered coculture with HDF cells below. This observation is in good agreement with previous studies on layered cocultures of fibroblasts and keratinocytes that reported robust cell viability and proliferation in collagen and fibrin constructs with PLA nanofibers,[58] on 3D sericin matrices,[85] collagen- or fibronectin-coated plates,[57] collagen hydrogels reinforced with a fibrin-coated PLLA nanofiber membrane,[61] and in collagen constructs.[56]

Previously, we have already reported an accelerated fibroblast migration cultivated in a monoculture on self-assembled fibrinogen nanofibers with respect to planar fibrinogen via 2D cell tracking.[45] Therefore, in the future, nanofibrous fibrinogen scaffolds with micrometer thickness[43] will be highly favorable to study 3D fibroblast infiltration into the fibrous network structure as also described in various 3D biomaterial constructs,[25,56,61] which is required to induce successful tissue regeneration during wound healing.[1]

Of the three fibrinogen topographies studied in this work, only fibrinogen nanofibers will be able to facilitate nutrient and oxygen supply to cells due to their porous architecture, which is another important requirement for wound healing.[1,86] More importantly, in contrast to planar fibrinogen, self-assembled fibrinogen nanofibers have a decisive technical advantage because they can be detached from the underlying substrate in aqueous solution to obtain free-standing scaffolds with tailored thickness.[43,45] Due to their flexible nature when rehydrated,[45] free-standing fibrinogen nanofibers could also become a very interesting scaffold type for other coculture systems and could for instance serve as innervated skin models[87] or could be developed into tubular constructs for artificial vascular grafts,[17] to replace seminiferous tubules[88] or to support peripheral nerve regeneration.[89] Combined with their good biocompatibility with fibroblast–keratinocyte cocultures, the possibility to use fibrinogen nanofibers as free-standing scaffolds will open the opportunity in the future to grow keratinocytes at an air–liquid interface (ALI) to promote cell differentiation and stratification, both being important features for successful wound closure.[3] Recently, successively layered cocultures as well as further growth at the ALI have already been reported for bioprinted 3D PCL/cellular dermal collagen scaffolds,[90] human skin organoids based on collagen-suspended stem cells,[78] and 3D-printed fibrin gels.[91] Based on this state of the art, self-assembled and detached fibrinogen nanofibers will in the future present the unique potential for cell seeding of fibroblasts and keratinocytes on either side of the scaffolds with further selective growth of keratinocytes at the ALI, to fabricate

a basal lamina model, similar to recently introduced stromal scaffolds from electrospun polymer fibers.[92]

## 5. CONCLUSIONS

In this study, we successfully established for the first time a coculture of human dermal fibroblasts (HDFs) and HaCaT keratinocytes as model skin cells on self-assembled fibrinogen nanofibers and flat fibrinogen topographies. The long-term viability of these cells was supported by fibrinogen nanofibers for 14 days compared with planar and physisorbed fibrinogen, both in mono- or coculture. Moreover, an overall higher proliferation rate over time and higher cellular metabolic activities at later time points were observed for cocultures in comparison to monocultures. The native morphology of both HDFs and HaCaTs, which strongly differed between the two cell types, was preserved on all fibrinogen topographies, and so was the native phenotype of fibroblasts and undifferentiated keratinocytes, indicated by expression of the cell-specific marker proteins vimentin and cytokeratin-14, respectively. A robust expression of fibronectin indicated a characteristic provisional ECM-secreting phenotype of fibroblasts. To later use fibrinogen scaffolds as biomimetic multilayered constructs resembling the native skin, a successive coculture of both cells was established on fibrinogen nanofibers and flat fibrinogen until 14 days, which yielded confluent HaCaT cells in the topmost layer with HDF cells below. Compared with planar and physisorbed fibrinogen scaffolds, self-assembled fibrinogen nanofiber scaffolds hold immense potential to serve as cell-free wound healing constructs because their porous architecture can facilitate nutrient and oxygen delivery and cell infiltration. Moreover, the unique possibility of fibrinogen nanofibers to be detached from an underlying substrate to serve as free-standing scaffolds will facilitate future studies of cell growth at an air–liquid interface that can mimic the native skin tissue microenvironment even more closely.

## ASSOCIATED CONTENT

### Supporting Information

The Supporting Information is available free of charge at https://pubs.acs.org/doi/10.1021/acsomega.2c07896.

Additional data on proliferation and viability, cytochemical staining, and cytoskeletal orientation of HDFs and HaCaTs on fibrinogen scaffolds as well as topography of physisorbed fibrinogen scaffolds (PDF)

## AUTHOR INFORMATION

### Corresponding Author

**Dorothea Brüggemann** − *Institute for Biophysics, University of Bremen, 28359 Bremen, Germany; MAPEX Center for Materials and Processes, University of Bremen, 28359 Bremen, Germany;* Present Address: City University of Applied Sciences, Neustadtswall 30, 28199 Bremen, Germany; orcid.org/0000-0002-7140-3275; Email: Dorothea.Brueggemann@hs-bremen.de

### Authors

**Arundhati Joshi** − *Institute for Biophysics, University of Bremen, 28359 Bremen, Germany*

**Titinun Nuntapramote** − *Institute for Biophysics, University of Bremen, 28359 Bremen, Germany*

Complete contact information is available at:
https://pubs.acs.org/10.1021/acsomega.2c07896

## REFERENCES

(1) Chouhan, D.; Dey, N.; Bhardwaj, N.; Mandal, B. B. Emerging and Innovative Approaches for Wound Healing and Skin Regeneration: Current Status and Advances. *Biomaterials* **2019**, *216*, 119267.

(2) Dreifke, M. B.; Jayasuriya, A. A.; Jayasuriya, A. C. Current Wound Healing Procedures and Potential Care. *Mater. Sci. Eng., C* **2015**, *48*, 651−662.

(3) Las Heras, K.; Igartua, M.; Santos-Vizcaino, E.; Hernandez, R. M. Chronic Wounds: Current Status, Available Strategies and Emerging Therapeutic Solutions. *J. Controlled Release* **2020**, *328*, 532−550.

(4) Rousselle, P.; Braye, F.; Dayan, G. Re-Epithelialization of Adult Skin Wounds: Cellular Mechanisms and Therapeutic Strategies. *Adv. Drug Delivery Rev.* **2019**, *146*, 344−365.

(5) Pastar, I.; Stojadinovic, O.; Yin, N. C.; Ramirez, H.; Nusbaum, A. G.; Sawaya, A.; Patel, S. B.; Khalid, L.; Isseroff, R. R.; Tomic-Canic, M. Epithelialization in Wound Healing: A Comprehensive Review. *Adv. Wound Care* **2014**, *3* (7), 445.

(6) Klicks, J.; von Molitor, E.; Ertongur-Fauth, T.; Rudolf, R.; Hafner, M. In Vitro Skin Three-Dimensional Models and Their Applications. *J. Cell. Biotechnol.* **2017**, *3* (1), 21−39.

(7) He, P.; Zhao, J.; Zhang, J.; Li, B.; Gou, Z.; Gou, M.; Li, X. Bioprinting of Skin Constructs for Wound Healing. *Burn. Trauma* **2018**, *6* (5), 1−10.

(8) Ng, W. L.; Qi, J. T. Z.; Yeong, W. Y.; Naing, M. W. Proof-of-Concept: 3D Bioprinting of Pigmented Human Skin Constructs. *Biofabrication* **2018**, *10* (2), 025005.

(9) Groeber, F.; Holeiter, M.; Hampel, M.; Hinderer, S.; Schenke-Layland, K. Skin Tissue Engineering - In Vivo and in Vitro Applications. *Adv. Drug Delivery Rev.* **2011**, *63*, 352−366.

(10) Gaharwar, A. K.; Singh, I.; Khademhosseini, A. Engineered Biomaterials for in Situ Tissue Regeneration. *Nat. Rev. Mater.* **2020**, *5* (9), 686−705.

(11) Yun, Y. E.; Jung, Y. J.; Choi, Y. J.; Choi, J. S.; Cho, Y. W. Artificial Skin Models for Animal-Free Testing. *J. Pharm. Investig.* *2018 482* **2018**, *48* (2), 215−223.

(12) Russo, B.; Brembilla, N. C.; Chizzolini, C. Interplay between Keratinocytes and Fibroblasts: A Systematic Review Providing a New Angle for Understanding Skin Fibrotic Disorders. *Front. Immunol.* **2020**, *11*, 1−20.

(13) Vig, K.; Chaudhari, A.; Tripathi, S.; Dixit, S.; Sahu, R.; Pillai, S.; Dennis, V. A.; Singh, S. R. Advances in Skin Regeneration Using Tissue Engineering. *Int. J. Mol. Sci. 2017, Vol. 18, Page 789* **2017**, *18* (4), 789.

(14) Yildirimer, L.; Thanh, N. T. K.; Seifalian, A. M. Skin Regeneration Scaffolds: A Multimodal Bottom-up Approach. *Trends Biotechnol.* **2012**, *30* (12), 638−648.

(15) Battiston, K. G.; Cheung, J. W. C.; Jain, D.; Santerre, J. P. Biomaterials in Co-Culture Systems: Towards Optimizing Tissue Integration and Cell Signaling within Scaffolds. *Biomaterials* **2014**, *35* (15), 4465−4476.

(16) Shafiee, S.; Shariatzadeh, S.; Zafari, A.; Majd, A.; Niknejad, H. Recent Advances on Cell-Based Co-Culture Strategies for Prevascularization in Tissue Engineering. *Front. Bioeng. Biotechnol.* **2021**, *9*, 1−20.

(17) Li, M.-X.; Li, L.; Zhou, S.-Y.; Cao, J.-H.; Liang, W.-H.; Tian, Y.; Shi, X.-T.; Yang, X.-B.; Wu, D.-Y. A Biomimetic Orthogonal-Bilayer Tubular Scaffold for the Co-Culture of Endothelial Cells and Smooth Muscle Cells. *RSC Adv.* **2021**, *11* (50), 31783−31790.

(18) Rajangam, T.; An, S. S. A. Fibrinogen and Fibrin Based Micro and Nano Scaffolds Incorporated with Drugs, Proteins, Cells and Genes for Therapeutic Biomedical Applications. *Int. J. Nanomedicine* **2013**, *8*, 3641.

(19) Suehiro, K.; Gailit, J.; Plow, E. F. Fibrinogen Is a Ligand for Integrin A5β1 on Endothelial Cells. *J. Biol. Chem.* **1997**, *272* (8), 5360−5366.

(20) Gailit, J.; Clarke, C.; Newman, D.; Tonnesen, M. G.; Mosesson, M. W.; Clark, R. A. F. Human Fibroblasts Bind Directly to Fibrinogen at RGD Sites through Integrin Avβ3. *Exp. Cell Res.* **1997**, *232* (1), 118−126.

(21) Joo, J. Y.; Amin, M. L.; Rajangam, T.; An, S. S. A. Fibrinogen as a Promising Material for Various Biomedical Applications. *Mol. Cell. Toxicol. 2015 111* **2015**, *11* (1), 1−9.

(22) Bhardwaj, N.; Chouhan, D.; Mandal, B. B. 3D Functional Scaffolds for Skin Tissue Engineering. *Funct. 3D Tissue Eng. Scaffolds Mater. Technol. Appl.* **2018**, 345−365.

(23) Ahmed, T. A. E.; Dare, E. V.; Hincke, M. Fibrin: A Versatile Scaffold for Tissue Engineering Applications. *Tissue Engineering Part B: Reviews* **2008**, *14* (2), 199−215.

(24) Weisel, J. W.; Litvinov, R. I. Fibrin Formation, Structure and Properties. *Sub-Cellular Biochemistry* **2017**, *82*, 405−456.

(25) Sun, T.; Haycock, J.; Macneil, S. In Situ Image Analysis of Interactions between Normal Human Keratinocytes and Fibroblasts Cultured in Three-Dimensional Fibrin Gels. *Biomaterials* **2006**, *27* (18), 3459−3465.

(26) Sese, N.; Cole, M.; Tawil, B. Proliferation of Human Keratinocytes and Cocultured Human Keratinocytes and Fibroblasts in Three-Dimensional Fibrin Constructs. *Tissue Eng. Part A* **2011**, *17* (3−4), 429−437.

(27) Sheikholeslam, M.; Wright, M. E. E.; Jeschke, M. G.; Amini-Nik, S. Biomaterials for Skin Substitutes. *Adv. Healthc. Mater.* **2018**, *7* (5), 1700897.

(28) Devolder, R.; Kong, H. J. Hydrogels for in Vivo-like Three-Dimensional Cellular Studies. *Wiley Interdiscip. Rev. Syst. Biol. Med.* **2012**, *4* (4), 351−365.

(29) Wnek, G. E.; Carr, M. E.; Simpson, D. G.; Bowlin, G. L. Electrospinning of Nanofiber Fibrinogen Structures. *Nano Lett.* **2003**, *3* (2), 213−216.

(30) Sell, S. A.; Francis, M. P.; Garg, K.; McClure, M. J.; Simpson, D. G.; Bowlin, G. L. Cross-Linking Methods of Electrospun Fibrinogen Scaffolds for Tissue Engineering Applications. *Biomedical Materials* **2008**, *3*, 045001.

(31) Keshvardoostchokami, M.; Majidi, S. S.; Huo, P.; Ramachandran, R.; Chen, M.; Liu, B. Electrospun Nanofibers of Natural and Synthetic Polymers as Artificial Extracellular Matrix for Tissue Engineering. *Nanomaterials* **2021**, *11* (1), 21.

(32) Yazdanpanah, A.; Madjd, Z.; Pezeshki-Modaress, M.; Khosrowpour, Z.; Farshi, P.; Eini, L.; Kiani, J.; Seifi, M.; Kundu, S. C.; Ghods, R.; et al. Bioengineering of Fibroblast-Conditioned Polycaprolactone/Gelatin Electrospun Scaffold for Skin Tissue Engineering. *Artif. Organs* **2022**, *46* (6), 1040−1054.

(33) Yuan, T. T.; DiGeorge Foushee, A. M.; Johnson, M. C.; Jockheck-Clark, A. R.; Stahl, J. M. Development of Electrospun Chitosan-Polyethylene Oxide/Fibrinogen Biocomposite for Potential Wound Healing Applications. *Nanoscale Res. Lett.* **2018**, *13* (1), 1−12.

(34) McManus, M. C.; Boland, E. D.; Simpson, D. G.; Barnes, C. P.; Bowlin, G. L. Electrospun Fibrinogen: Feasibility as a Tissue Engineering Scaffold in a Rat Cell Culture Model. *J. Biomed. Mater. Res. - Part A* **2007**, *81A* (2), 299−309.

(35) Gugutkov, D.; Gustavsson, J.; Ginebra, M. P.; Altankov, G. Fibrinogen Nanofibers for Guiding Endothelial Cell Behavior. *Biomater. Sci.* **2013**, *1*, 1065−1073.

(36) McManus, M.; Boland, E.; Sell, S.; Bowen, W.; Koo, H.; Simpson, D.; Bowlin, G. Electrospun Nanofibre Fibrinogen for Urinary Tract Tissue Reconstruction. *Biomed. Mater.* **2007**, *2*, 257−262.

(37) Nedjari, S.; Awaja, F.; Altankov, G. Three Dimensional Honeycomb Patterned Fibrinogen Based Nanofibers Induce Sub-stantial Osteogenic Response of Mesenchymal Stem Cells. *Sci. Reports 2017 71* **2017**, *7* (1), 1−11.

(38) Forget, J.; Awaja, F.; Gugutkov, D.; Gustavsson, J.; Gallego Ferrer, G.; Coelho-Sampaio, T.; Hochman-Mendez, C.; Salmeron-Sánchez, M.; Altankov, G. Differentiation of Human Mesenchymal Stem Cells Toward Quality Cartilage Using Fibrinogen-Based Nanofibers. *Macromol. Biosci.* **2016**, *16*, 1348−1359.

(39) Mirzaei-Parsa, M. J.; Ghanbari, H.; Bahrami, N.; Hadadi-Abianeh, S.; Faridi-Majidi, R. The Effects of Cross-Linked/Uncross-Linked Electrospun Fibrinogen/Polycaprolactone Nanofibers on the Proliferation of Normal Human Epidermal Keratinocytes. *J. Polym. Eng.* **2018**, *38* (10), 945−953.

(40) Palchesko, R. N.; Sun, Y.; Zhang, L.; Szymanski, J. M.; Jallerat, Q.; Feinberg, A. W. Nanofiber Biomaterials. In *Springer Handbook of Nanomaterials*; Springer: Berlin, 2013; pp 977−1010. DOI: 10.1007/978-3-642-20595-8_27.

(41) Barnes, C. P.; Sell, S. A.; Boland, E. D.; Simpson, D. G.; Bowlin, G. L. Nanofiber Technology: Designing the next Generation of Tissue Engineering Scaffolds. *Adv. Drug Delivery Rev.* **2007**, *59* (14), 1413−1433.

(42) Raoufi, M.; Aslankoohi, N.; Mollenhauer, C.; Boehm, H.; Spatz, J. P.; Brüggemann, D. Template-Assisted Extrusion of Biopolymer Nanofibers under Physiological Conditions. *Integr. Biol.* **2016**, *8* (10), 1059−1066.

(43) Stapelfeldt, K.; Stamboroski, S.; Mednikova, P.; Brüggemann, D. Fabrication of 3D-Nanofibrous Fibrinogen Scaffolds Using Salt-Induced Self Assembly. *Biofabrication* **2019**, *11*, 025010.

(44) Stapelfeldt, K.; Stamboroski, S.; Walter, I.; Suter, N.; Kowalik, T.; Michaelis, M.; Brüggemann, D. Controlling the Multiscale Structure of Nanofibrous Fibrinogen Scaffolds for Wound Healing. *Nano Lett.* **2019**, *19*, 6554.

(45) Suter, N.; Joshi, A.; Wunsch, T.; Graupner, N.; Stapelfeldt, K.; Radmacher, M.; Müssig, J.; Brüggemann, D. Self-Assembled Fibrinogen Nanofibers Support Fibroblast Adhesion and Prevent E. Coli Infiltration. *Mater. Sci. Eng., C* **2021**, *126*, 112156.

(46) Kenny, M.; Stamboroski, S.; Taher, R.; Brüggemann, D.; Schoen, I. Nanofiber Topographies Enhance Platelet-Fibrinogen Scaffold Interactions. *Adv. Healthc. Mater.* **2022**, *11* (14), 2200249.

(47) Dutta, D.; Markhoff, J.; Suter, N.; Rezwan, K.; Brüggemann, D. Effect of Collagen Nanofibers and Silanization on the Interaction of HaCaT Keratinocytes and 3T3 Fibroblasts with Alumina Nanopores. *ACS Appl. Bio Mater.* **2021**, *4* (2), 1852−1862.

(48) Rao, K. M.; Suneetha, M.; Park, G. T.; Babu, A. G.; Han, S. S. Hemostatic, Biocompatible, and Antibacterial Non-Animal Fungal Mushroom-Based Carboxymethyl Chitosan-ZnO Nanocomposite for Wound-Healing Applications. *Int. J. Biol. Macromol.* **2020**, *155*, 71−80.

(49) Narayanan, K. B.; Zo, S. M.; Han, S. S. Novel Biomimetic Chitin-Glucan Polysaccharide Nano/Microfibrous Fungal-Scaffolds for Tissue Engineering Applications. *Int. J. Biol. Macromol.* **2020**, *149*, 724−731.

(50) Salas-Oropeza, J.; Jimenez-Estrada, M.; Perez-Torres, A.; Castell-Rodriguez, A. E.; Becerril-Millan, R.; Rodriguez-Monroy, M. A.; Canales-Martinez, M. M. Wound Healing Activity of the Essential Oil of Bursera Morelensis, in Mice. *Molecules* **2020**, *25* (8), 1795.

(51) Rueden, C. T.; Eliceiri, K. W. ImageJ for the Next Generation of Scientific Image Data. *Microsc. Microanal.* **2019**, *25* (S2), 142−143.

(52) Trescher, K.; Roch, T.; Cui, J.; Kratz, K.; Lendlein, A.; Jung, F. Test System for Evaluating the Influence of Polymer Properties on Primary Human Keratinocytes and Fibroblasts in Mono- and Coculture. *J. Biotechnol.* **2013**, *166* (1−2), 58−64.

(53) Lammers, G.; Tjabringa, G. S.; Schalkwijk, J.; Daamen, W. F.; van Kuppevelt, T. H. A Molecularly Defined Array Based on Native Fibrillar Collagen for the Assessment of Skin Tissue Engineering Biomaterials. *Biomaterials* **2009**, *30* (31), 6213−6220.

(54) Colombo, I.; Sangiovanni, E.; Maggio, R.; Mattozzi, C.; Zava, S.; Corbett, Y.; Fumagalli, M.; Carlino, C.; Corsetto, P. A.; Scaccabarozzi, D.; Calvieri, S.; Gismondi, A.; Taramelli, D.; Dell'Agli, M. HaCaT Cells as a Reliable In Vitro Differentiation

Model to Dissect the Inflammatory/Repair Response of Human Keratinocytes. *Mediators Inflamm.* **2017**, *2017*, 7435621.

(55) To, W. S.; Midwood, K. S. Plasma and Cellular Fibronectin: Distinct and Independent Functions during Tissue Repair. *Fibrogenes. Tissue Repair 2011 41* **2011**, *4* (1), 1−17.

(56) Iyer, K.; Chen, Z.; Ganapa, T.; Wu, B. M.; Tawil, B.; Linsley, C. S. Keratinocyte Migration in a Three-Dimensional In Vitro Wound Healing Model Co-Cultured with Fibroblasts. *Tissue Eng. Regen. Med.* **2018**, *15* (6), 721−733.

(57) Wang, Z.; Wang, Y.; Farhangfar, F.; Zimmer, M.; Zhang, Y. Enhanced Keratinocyte Proliferation and Migration in Co-Culture with Fibroblasts. *PLoS One* **2012**, *7* (7), e40951.

(58) Law, J. X.; Musa, F.; Ruszymah, B. H. I.; El Haj, A. J.; Yang, Y. A Comparative Study of Skin Cell Activities in Collagen and Fibrin Constructs. *Med. Eng. Phys.* **2016**, *38* (9), 854−861.

(59) Sun, T.; Mai, S.; Norton, D.; Haycock, J. W.; Ryan, A. J.; Macneil, S. Self-Organization of Skin Cells in Three-Dimensional Electrospun Polystyrene Scaffolds. *Tissue Eng.* **2005**, *11* (7−8), 1023− 1033.

(60) Kempf, M.; Miyamura, Y.; Liu, P. Y.; Chen, A. C. H.; Nakamura, H.; Shimizu, H.; Tabata, Y.; Kimble, R. M.; McMillan, J. R. A Denatured Collagen Microfiber Scaffold Seeded with Human Fibroblasts and Keratinocytes for Skin Grafting. *Biomaterials* **2011**, *32* (21), 4782−4792.

(61) Bacakova, M.; Pajorova, J.; Broz, A.; Hadraba, D.; Lopot, F.; Zavadakova, A.; Vistejnova, L.; Beno, M.; Kostic, I.; Jencova, V.; et al. A Two-Layer Skin Construct Consisting of a Collagen Hydrogel Reinforced by a Fibrin-Coated Polylactide Nanofibrous Membrane. *Int. J. Nanomedicine* **2019**, *14*, 5033−5050.

(62) Chester, D.; Brown, A. C. The Role of Biophysical Properties of Provisional Matrix Proteins in Wound Repair. *Matrix Biol.* **2017**, *60− 61*, 124−140.

(63) Kubo, M.; Van De Water, L.; Plantefaber, L. C.; Mosesson, M. W.; Simon, M.; Tonnesen, M. G.; Taichman, L.; Clark, R. A. F. Fibrinogen and Fibrin Are Anti-Adhesive for Keratinocytes: A Mechanism for Fibrin Eschar Slough During Wound Repair. *J. Invest. Dermatol.* **2001**, *117* (6), 1369−1381.

(64) Yamamoto, M.; Yanaga, H.; Nishina, H.; Watabe, S.; Mamba, K. Fibrin Stimulates the Proliferation of Human Keratinocytes through the Autocrine Mechanism of Transforming Growth Factor-Alpha and Epidermal Growth Factor Receptor. *Tohoku J. Exp. Med.* **2005**, *207* (1), 33−40.

(65) Solovieva, E. V.; Fedotov, A. Y.; Mamonov, V. E.; Komlev, V. S.; Panteleyev, A. A. Fibrinogen-Modified Sodium Alginate as a Scaffold Material for Skin Tissue Engineering. *Biomed. Mater.* **2018**, *13* (2), 025007.

(66) Blanquer, A.; Musilkova, J.; Filova, E.; Taborska, J.; Brynda, E.; Riedel, T.; Klapstova, A.; Jencova, V.; Mullerova, J.; Kostakova, E. K.; et al. The Effect of a Polyester Nanofibrous Membrane with a Fibrin-Platelet Lysate Coating on Keratinocytes and Endothelial Cells in a Co-Culture System. *Nanomaterials* **2021**, *11* (2), 457.

(67) Weiss, E.; Yamaguchi, Y.; Falabella, A.; Crane, S.; Tokuda, Y.; Falanga, V. Un-Cross-Linked Fibrin Substrates Inhibit Keratinocyte Spreading and Replication: Correction with Fibronectin and Factor XIII Cross-Linking. *J. Cell. Physiol.* **1998**, *174* (1), 58−65.

(68) Geer, D. J.; Andreadis, S. T. A Novel Role of Fibrin in Epidermal Healing: Plasminogen-Mediated Migration and Selective Detachment of Differentiated Keratinocytes. *J. Invest. Dermatol.* **2003**, *121* (5), 1210−1216.

(69) Behm, B.; Babilas, P.; Landthaler, M.; Schreml, S. Cytokines, Chemokines and Growth Factors in Wound Healing. *J. Eur. Acad. Dermatology Venereol.* **2012**, *26* (7), 812−820.

(70) Spiekstra, S. W.; Breetveld, M.; Rustemeyer, T.; Scheper, R. J.; Gibbs, S. Wound-Healing Factors Secreted by Epidermal Keratinocytes and Dermal Fibroblasts in Skin Substitutes. *Wound Repair Regen.* **2007**, *15* (5), 708−717.

(71) Werner, S.; Krieg, T.; Smola, H. Keratinocyte−Fibroblast Interactions in Wound Healing. *J. Invest. Dermatol.* **2007**, *127* (5), 998−1008.

(72) Mh Busra, F.; Lokanathan, Y.; Mohd Nadzir, M.; Saim, A.; Hj Idrus, R.; Chowdhury, S. R. Attachment, Proliferation, and Morphological Properties of Human Dermal Fibroblasts on Ovine Tendon Collagen Scaffolds: A Comparative Study. *Malays. J. Med. Sci.* **2017**, *24* (2), 33.

(73) Jalal, S.; Shi, S.; Acharya, V.; Huang, R. Y. J.; Viasnoff, V.; Bershadsky, A. D.; Tee, Y. H. Actin Cytoskeleton Self-Organization in Single Epithelial Cells and Fibroblasts under Isotropic Confinement. *J. Cell Sci.* **2019**, *132* (5), 1−14.

(74) Koehler, M. J.; Zimmermann, S.; Springer, S.; Elsner, P.; König, K.; Kaatz, M. Keratinocyte Morphology of Human Skin Evaluated by in Vivo Multiphoton Laser Tomography. *Skin Res. Technol.* **2011**, *17* (4), 479−486.

(75) Chen, H.; Lui, Y. S.; Tan, Z. W.; Lee, J. Y. H.; Tan, N. S.; Tan, L. P. Migration and Phenotype Control of Human Dermal Fibroblasts by Electrospun Fibrous Substrates. *Adv. Healthc. Mater.* **2019**, *8* (9), 1801378.

(76) Pajoum Shariati, S. R.; Shokrgozar, M. A.; Vossoughi, M.; Eslamifar, A. In Vitro Co-Culture of Human Skin Keratinocytes and Fibroblasts on a Biocompatible and Biodegradable Scaffold. *Iran. Biomed. J.* **2009**, *13* (3), 169−177.

(77) Zoio, P.; Ventura, S.; Leite, M.; Oliva, A. Pigmented Full-Thickness Human Skin Model Based on a Fibroblast-Derived Matrix for Long-Term Studies. *Tissue Eng. - Part C Methods* **2021**, *27* (7), 433−443.

(78) Kim, Y.; Park, N.; Rim, Y. A.; Nam, Y.; Jung, H.; Lee, K.; Ju, J. H. Establishment of a Complex Skin Structure via Layered Co-Culture of Keratinocytes and Fibroblasts Derived from Induced Pluripotent Stem Cells. *Stem Cell Res. Ther.* **2018**, *9* (1), 1−10.

(79) Robinson-Bennett, B.; Han, A. 30 Role of Immunohistochemistry in Elucidating Lung Cancer Metastatic to the Ovary from Primary Ovarian Carcinoma. In *Handbook of Immunohistochemistry and in Situ Hybridization of Human Carcinomas*; Academic Press, 2005; Vol. 4, pp 537−545. DOI: 10.1016/S1874-5784(05)80116-3.

(80) Dulbecco, R.; Elkington, J. Induction of Growth in Resting Fibroblastic Cell Cultures by Ca++. *Proc. Natl. Acad. Sci. U. S. A.* **1975**, *72* (4), 1584.

(81) Tomasek, J. J.; Gabbiani, G.; Hinz, B.; Chaponnier, C.; Brown, R. A. Myofibroblasts and Mechano-Regulation of Connective Tissue Remodelling. *Nat. Rev. Mol. Cell Biol. 2002 35* **2002**, *3* (5), 349−363.

(82) Fleischmajer, R.; MacDonald, E. D.; Contard, P.; Perlish, J. S. Immunochemistry of a Keratinocyte-Fibroblast Co-Culture Model for Reconstruction of Human Skin. *J. Histochem. Cytochem.* **1993**, *41* (9), 1359−1366.

(83) Harrison, C. A.; Dalley, A. J.; Mac Neil, S. A Simple in Vitro Model for Investigating Epithelial/Mesenchymal Interactions: Keratinocyte Inhibition of Fibroblast Proliferation and Fibronectin Synthesis. *Wound Repair Regen.* **2005**, *13* (6), 543−550.

(84) Stark, H. J.; Willhauck, M. J.; Mirancea, N.; Boehnke, K.; Nord, I.; Breitkreutz, D.; Pavesio, A.; Boukamp, P.; Fusenig, N. E. Authentic Fibroblast Matrix in Dermal Equivalents Normalises Epidermal Histogenesis and Dermo-Epidermal Junction in Organotypic Co-Culture. *Eur. J. Cell Biol.* **2004**, *83* (11−12), 631−645.

(85) Nayak, S.; Dey, S.; Kundu, S. C. Skin Equivalent Tissue-Engineered Construct: Co-Cultured Fibroblasts/ Keratinocytes on 3D Matrices of Sericin Hope Cocoons. *PLoS One* **2013**, *8* (9), e74779.

(86) Mayet, N.; Choonara, Y. E.; Kumar, P.; Tomar, L. K.; Tyagi, C.; Du Toit, L. C.; Pillay, V. A Comprehensive Review of Advanced Biopolymeric Wound Healing Systems. *J. Pharm. Sci.* **2014**, *103* (8), 2211−2230.

(87) Schutte, S. C.; Kadakia, F.; Davidson, S. Skin-Nerve Co-Culture Systems for Disease Modeling and Drug Discovery. *Tissue Eng. - Part C Methods* **2021**, *27* (2), 89−99.

(88) Vardiani, M.; Ghaffari Novin, M.; Koruji, M.; Nazarian, H.; Goossens, E.; Aghaei, A.; Seifalian, A. M.; Ghasemi Hamidabadi, H.; Asgari, F.; Gholipourmalekabadi, M. Gelatin Electrospun Mat as a Potential Co-Culture System for in Vitro Production of Sperm Cells

from Embryonic Stem Cells. *ACS Biomater. Sci. Eng.* **2020**, *6* (10), 5823−5832.

(89) Muangsanit, P.; Roberton, V.; Costa, E.; Phillips, J. B. Engineered Aligned Endothelial Cell Structures in Tethered Collagen Hydrogels Promote Peripheral Nerve Regeneration. *Acta Biomater.* **2021**, *126*, 224−237.

(90) Ramasamy, S.; Davoodi, P.; Vijayavenkataraman, S.; Teoh, J. H.; Thamizhchelvan, A. M.; Robinson, K. S.; Wu, B.; Fuh, J. Y. H.; DiColandrea, T.; Zhao, H.; et al. Optimized Construction of a Full Thickness Human Skin Equivalent Using 3D Bioprinting and a PCL/ Collagen Dermal Scaffold. *Bioprinting* **2021**, *21*, e00123.

(91) Zhou, Y.; Fan, Y.; Chen, Z.; Yue, Z.; Wallace, G. Catechol Functionalized Ink System and Thrombin-Free Fibrin Gel for Fabricating Cellular Constructs with Mechanical Support and Inner Micro Channels. *Biofabrication* **2022**, *14* (1), 015004.

(92) Weigel, T.; Malkmus, C.; Weigel, V.; Wußmann, M.; Berger, C.; Brennecke, J.; Groeber-Becker, F.; Hansmann, J.; et al. Fully Synthetic 3D Fibrous Scaffolds for Stromal Tissues—Replacement of Animal-Derived Scaffold Materials Demonstrated by Multilayered Skin. *Adv. Mater.* **2022**, *34*, 2106780.